Modulation of the Molecular Structure of Tri-aryl Amine Fibrils in Hybrid Poly[vinyl chloride] Gel/Organogel Systems

Parniyan Talebpour, Benoît Heinrich, Odile Gavat, Alain Carvalho, Emilie Moulin, Nicolas Giuseppone, Jean-Michel Guenet

MODULATION OF THE MOLECULAR STRUCTURE OF TRI-ARYL AMINE FIBRILS IN HYBRID POLY[VINYL CHLORIDE] GEL/ORGANOGEL SYSTEMS.

TALEBPOUR[1], Parniyan; HEINRICH[2], Benoît; GAVAT[1], Odile; CARVALHO[1], Alain; MOULIN[1], Emilie; GIUSEPPONE[1], Nicolas; GUENET[1], Jean-Michel.*

1 Institut Charles Sadron
CNRS-Université de Strasbourg
23 rue du Loess, BP84047
67034 STRASBOURG, Cedex2, France

2 IPCMS
Université de Strasbourg-CNRS
23 rue du Loess, BP 43
67034, STRASBOURG Cedex 2, France

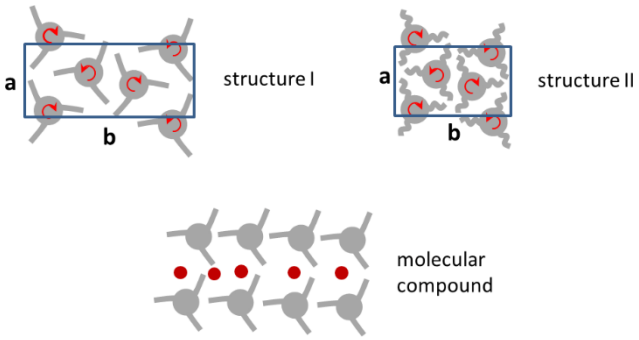

Graphical abstract legend: different TATA helix packings in the bulk and in the gel state

Corresponding author: Jean-Michel GUENET **jean-michel.guenet@ics-cnrs.unistra.fr**

Keywords : hybrid materials, PVC, thermoreversible gels, organogels, arylamines

Abstract: This paper reports on the thermodynamics through the mapping out of temperature-concentration phase diagrams, as well as the molecular structure and the morphology of binary organogels prepared from tris-amide triarylamine (TATA) in tetrachloroetane, and on their ternary thermoreversible hybrid gels formed with polyvinyl chloride. For low PVC contents the TATA organogel moiety behaves as in the binary systems, while for higher PVC contents the thermal behaviour is significantly altered with the appearance of a non-variant event. The molecular structure of the TATA assemblies is compared with those observed in the bulk solid state. Three molecular packings are observed in the bulk, whose crystalline lattices are tentatively derived. Structure I obtained after the crystallization-purification process, and is seen to transform at higher temperature into structure II. By cooling structure III is obtained which transforms reversibly into structure II on heating. The metastability of structure I leads on to contemplate the possible formation of molecular compounds during the crystallization-purification process in the presence of chlorinated solvents, the more so as the crystalline structures in the gels turns out to exhibit high similarities.

Finally, the morphology observation reveals that the TATA fibrils and the PVC matrix can be well identified for low PVC contents while for higher PVC content one essentially observes the TATA fibrils.

INTRODUCTION

The introduction of additives in polymers is a classical process, which is widely used in the aim of improving their properties, such as enhancing the mechanical properties, preventing from degradation, and the like [1]. Usage properties can also be improved by chemical modification such as cross-linking (vulcanization for instance). Another aspect of interest consists in imparting a functional property to a common polymer in order to transform it to a value-added material for more sophisticated purposes.

These past 20 years a wealth of organic molecules bearing functional properties, designated as gelators, have been synthesized by organic chemists [2-4]. These molecules can form thermoreversible gels, namely organogels, in a large variety of organic solvents. Based on this capability, Guenet and coworkers have succeeded in designing polymer-based functional materials through the formation of hybrid thermoreversible gels by means of a common solvent [5-10]. The function-bearing organogel pervades the polymer gel, while still preserving its original functional property or even displaying a new and unexpected behavior such as unusual magnetic properties[8].

Among the wealth of functional organogelators, triarylamine derivatives [11-13]and more particularly tris-amide triarylamines (TATA) are of particular interest thanks to their high conductivity properties [14,17]. We have recently succeeded in obtaining PVC-based materials with this type of organogelators [15]. PVC (Polyvinyl chloride), is the third-most manufactured synthetic polymer with use in plumbing, floor covering, textiles, and the like. An interesting, and quite unique property of this polymer lies in its propensity of producing thermoreversible gels in a large variety of solvents [18-25]. PVC-made textiles are obtained by spinning a gel formed in a mixture of solvents. Devising materials from this polymer with improved and/or new properties may have therefore potential applications in textile fibers[5] and/or porous materials[6].

Herein, as part of our investigations on these PVC/organogels materials, we report on the structure investigation of the TATA molecules in the hybrid gels with PVC that are prepared from 1,1,2,2-tetrachlorethane, a solvent wherein TATA fibrils display high conductivity. We particularly show

that the assembled TATA molecules exhibit several molecular structures both in the solid state and in the hybrid gels.

EXPERIMENTAL SECTION

Materials

The PVC used in the present study was purchased from Sigma-Aldrich and was used as-received. The weight average molecular weight as determined by SEC in THF at 25°C (universal calibration) is M_w= 7.9x10^4 g/mol and the polydispersity index M_w/M_n=1.87. The fractions of tetrads obtained by 13C-NMR are: sss=41% ssi, iss, sis,…= 39% and iii= 19%.

The fibrillar organogels were obtained from solutions of *tri-aryl tri-amines* designated as TATA in what follows (see figure 1). The synthesis and properties of these molecules are extensively described in references 11-17.

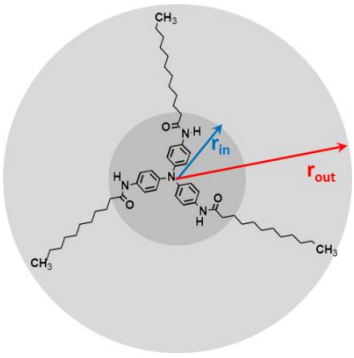

Figure 1: *Chemical structure of the tris-amide triarylamine TATA-C11 in its completely extended conformation, which can be inscribed in a cylinder of radius r_{out}. The circular domain defined by r_{in} possesses a higher electron density than the outer corona. $r_{out} \approx$ 2 nm and $r_{in} \approx$ 0.83 nm. Owing to steric hindrance, the phenyl rings are actually tilted so that this molecule differs from its mirror image.*

1,1,2,2-tetrachloroethane (TCE), from SigmaAldrich (purity grade 99.5%), was used throughout this study without further purification. This solvent was chosen because TATA gels from display high conductivity[26]

The preparation of the binary gels (PVC/TCE, TATA/TCE) and of the hybrid networks (PVC/TATA/TCE) is quite straightforward: mixtures are prepared at the desired concentration, and then heated up to 120-140°C until clear, homogeneous solutions are obtained. These solutions are quenched at low temperature (0°C down to -20°C) for producing the gels.

Four PVC concentrations have been studied: 4.82×10^{-2} g/cm^3 (or $3.0\text{x}10^{-2}$ in g/g), designated as PVC5%, 9.3×10^{-2} g/cm^3 (or $5.8\text{x}10^{-2}$ in g/g) designated as PVC10%, 0.17 g/cm^3 (or 0.11 in g/g) designated as PVC20%, and 0.246 g/cm^3 (or 0.158 in g/g) designated as PVC30%. TATA concentration was varied from 0.5×10^{-2} g/cm^3 (or 0.004 g/g) to 1.04×10^{-2} g/cm^3 (or 0.065 g/g).

Differential Scanning Calorimetry

A DSC 8500 from Perkin Elmer has been used for determining the gel formation, the gel melting temperatures, as well as the corresponding enthalpies of the TATA moiety. Three heating and cooling rates were used, namely 5°C/min, 10°C/min and 15°C/min within a temperature range from -20°C to 140°C.

Although gel formation arises from the crystallization of the longest syndiotactic sequences, the thermal behaviour of PVC gels cannot be observed by DSC (see sup.info. figure S1) as has been already reported in several papers [24,25]. Only the first run gives the melting range, yet the enthalpy is highly overestimated (see sup.info. figure S1). This implies that PVC gel formation cannot be determined by this technique. The tube tilting method has been used instead (see sup.info. figure S2).

Samples containing TATA were prepared as described above. About 30-40 mg of gel were introduced into stainless steel pans that were hermetically sealed by means of an o-ring. A first run was systematically performed for erasing the sample history, as well as to suppress parasitic mechanical effects at the gel melting [25]. The weight of the sample was systematically checked after the different cycles in order to evaluate any solvent loss.

Scanning Electron Microscopy

A piece of a gel from PVC/TCE or PVC/TATA/TCE was placed onto a cryo-holder and quickly plunged into a nitrogen slush. After transferring the sample under vacuum into the Quorum PT3010 chamber attached to the microscope, the frozen sample was coated with a thin Pt layer by sputter deposition, and was fractured with a razor blade. Subsequent etching was carried out at T=-70°C so as to reveal the details of the morphology. Samples were eventually transferred in the FEG-

cryoSEM (Hitachi SU8010) and observed at 1keV and at T=-150°C. The images were taken with the SE-in lens detector.

X-ray diffraction

The diffraction patterns were obtained with a transmission Guinier-like geometry. A linear focalized monochromatic Cu Kα1 beam (λ = 1.54056 Å) was obtained using an Inel XRG2500 sealed-tube generator (600W) equipped with a bent quartz monochromator. The samples were filled in home-made sealed cells of adjustable thickness. Sample temperature was controlled within 0.3°C and acquisition times were of 24h or 48h. The patterns were recorded on image plates and scanned by Amersham Typhoon IP with 25 µm resolution. I(q) profiles were obtained from images, by using home-developed software.

RESULTS AND DISCUSSION

1) The tri-aryl-triamine molecules

Characterization of the TATA molecules in the solid state has been achieved on samples purified by a slow recrystallization process from solution in acetone/dichloromethane mixed solvents (70/30 v/v). The DSC thermogram performed on this as-received sample displays several endotherms. Yet, after the first heating-cooling cycle two well-defined, reproducible endotherms are observed at T= 198°C and T= 222°C, respectively (see figure 2a). These outcomes arise from differing crystalline structures as revealed by the X-ray diffraction patterns in figure 3a.

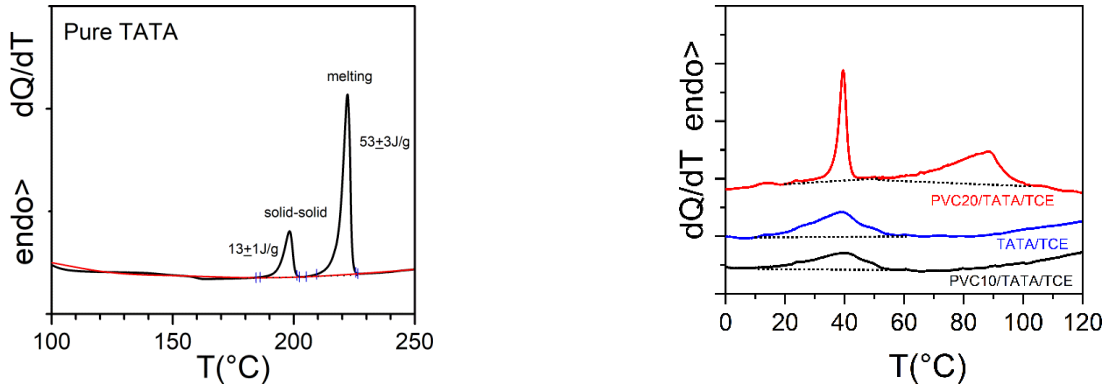

Figure 2: a) *left*: *DSC trace for pure TATA. Heating rate 5°C/min; b) right DSC traces for gels in different systems as indicated,* C_{TATA}*= 0.02g/cm*^{3}.

The structure of the as-received sample (*structure I*) displays three strong reflections corresponding to distances of 2.6 nm, 1.97 nm and 1.86 nm, as calculated by means of Bragg's law, as well as other minor reflections (figure S3 in supp.info.). Once the sample is heated at 200°C, the diffraction pattern is totally altered (*structure II*). Three strong reflections are also seen but corresponding to distances of 2.86 nm, 1.73 nm and 1.43 nm. In addition, there is the appearance of a conspicuous amorphous halo centered on the first peak. All the peaks observed at this temperature are significantly narrower than those see on the as-received sample, which implies a larger long-order range. The diffraction pattern recorded at room temperature differs totally (*structure III*), and shows three major peaks at distances of 2.35 nm, 1.63 nm, and 1.14 nm that are also much broader than those observed at 200°C.

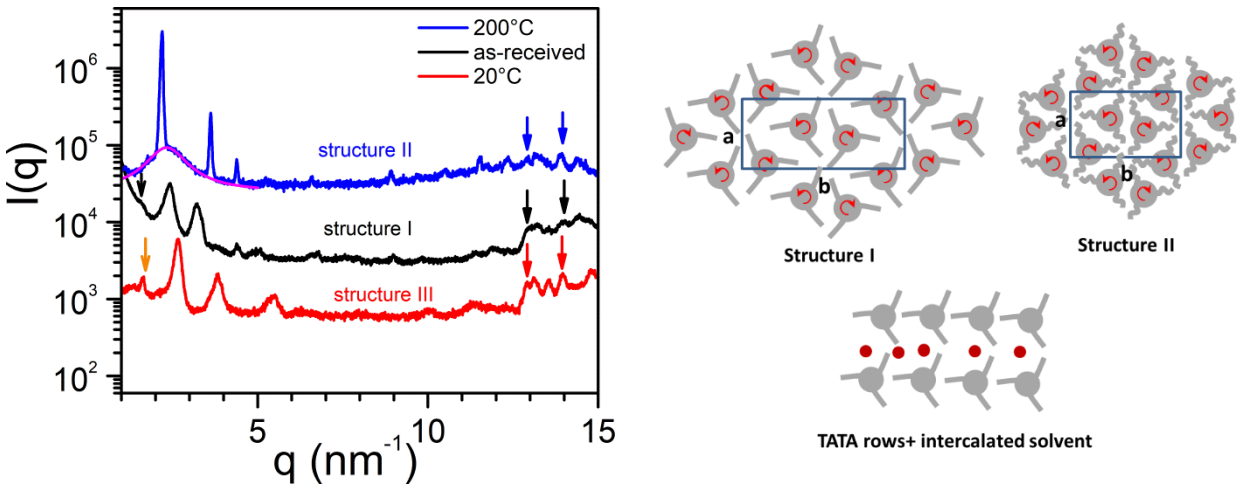

Figure 3: a) ***left***: *diffraction patterns of TATA in the solid state; Small peaks at low q are highlighted by arrows, peaks at larger q corresponding to the helix elevation (h= 0.48 nm) and to the spacing between phenyls of adjacent molecules are also shown, see text for further explanation. The pink line highlights the appearance of an amorphous halo. b)* ***right****: tentative 2D crystalline lattices, the grey objects are schematized version of the TATA molecules. The red arrows indicate the left-handed and right-handed helices. In structure II the aliphatic arms are disorganized. Structure III could not be solved and is possibly a superimposition of different states. The lower right structure involves row of TATA molecules encompassing solvent molecules, thus forming clathrates. This sketch does not bear any further meaning as to the placement of the molecules and their number per TATA molecule.*

Th

corresponds to a solid-solid transformation (*structure III* ⇒ *structure II*); ii) this transformation is reversible on cooling (*structure II* ⇒ *structure III*); iii) *structure I* is due to the recrystallization-purification process, and is erased when heating at 200°C. This accounts for the complex DSC trace observed on the first heating. As will be discussed below, this possibly relates to the formation of molecular compounds between the TATA molecules and the solvent. One common feature of the three diffraction patterns is the occurrence at larger q of reflections at d= 0.48 nm and 0.45 nm (see figure 3a). According to reference 16, TATA molecules stack onto one another while rotating by 18°, thus generating a 20_1 helix with a pitch of about 10 nm. The 18° rotation from one molecule to the next arises from the fact that the TATA molecule as mentioned in the legend of figure 1 is not strictly planar, the three phenyl groups being tilted due to steric hindrance. These values correspond to the elevation of the helical structure, h= 0.484 nm, as calculated by DFT, and to the distance of the phenyl groups of adjacent TATA molecules (0.45), respectively[16]. The diffraction peaks at lower q relate to the packing of the TATA helices.

Deriving crystalline lattice with only a few numbers of reflections together with the absence of oriented samples is usually difficult. Here we shall propose tentative crystalline lattices on the basis of an analogy with the diffraction patterns published on stereoregular polyolefins [27,28]. To be sure, the lack of oriented samples entails that only a two-dimensional lattice can be suggested, namely how helices pack together. As is customary, **c** will stand as the helical axis, corresponding to Miller index *l*. We shall therefore only consider *hk0* planes and so only attempt to determine the values of **a** and **b** axes.

First, one should realize that the TATA molecule exhibits chirality in the sense that it differs from its mirror image, and it further possesses a threefold symmetry (see figure 1). Consequently, one must observe the occurrence of both *right-handed* and *left-handed* helices, while the threefold symmetry will play a major role independent of the actual helical structure.

In the case of structure I, the pattern could be indexed in an orthorhombic lattice of parameters a= 2.78 nm, b= 7.85 nm and γ= 90° (see table S1 in supp. info). Intensity ratios and lattice size indicate an arrangement of 4 molecular chains analogue to that of isotactic polypropylene chains (see figure 3b).[27] However, the in-plane structure deviates from reference polymer by the symmetry changing from c2mm to P2gg or lower, as demonstrated by the presence of a weak reflection (230) that does not fulfill the condition h+k= 2n. Reason is obviously the asymmetric TATA molecule shape resulting in small shifts between neighboring rows of molecular chains, as represented in figure 3b. Note that this structure is not reformed from the solid state after transformation into structure II. It is suspected that it may arise from the formation of TATA/solvent molecular compound whose crystal structure remains unaltered after solvent removal, an effect already reported in the case of syndiotactic polystyrene for the so-called δ form [29]. This δ form structure does not reform after melting as observed here[29]. The fact that the structure in TATA/bromobenzene gels differs from that in TCE is a strong indication of the presence of the solvent within the crystalline lattice.

The structure of isotactic polystyrene seems relevant to account for the diffraction pattern of *structure II* [28]. On this basis we can derive lattice parameters $a = 3.47$ nm, $b = 5.03$ nm, $\gamma = 90°$.

(figure 3b, and table S2 in supp. Info.). Interestingly, the maximum of the broad amorphous halo seen at low q coincides with the *110* direction. This plane contains the aliphatic arms of the TATA molecules in the proposed lattice, which are therefore disorganized as further confirmed by the appearance of a scattering halo at 14 nm^{-1} related to their lateral distance. The transformation observed by DSC at T= 198°C is therefore triggered by the "melting" of the aliphatic arms.

It has not been possible to derive a crystalline lattice for *structure III*. It is suspected that it is a superimposition of different forms after the reorganization of the aliphatic arms. Note that the ratio

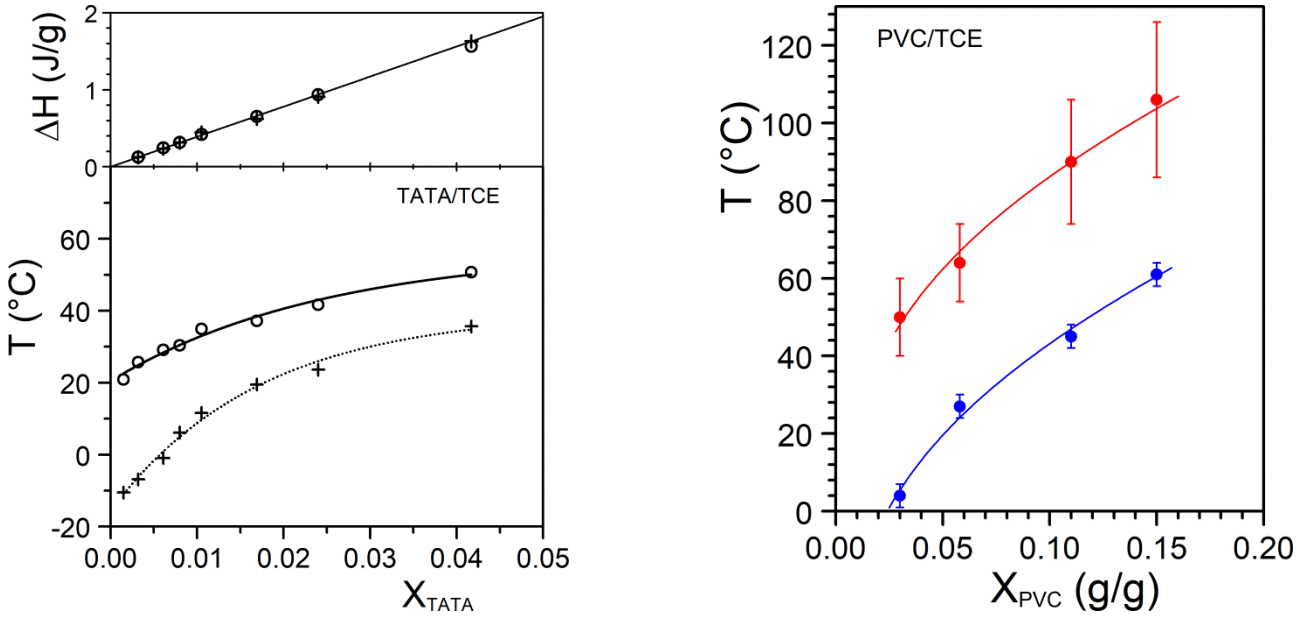

Figure 4: a) ***left***: *Temperature-concentration phase diagram TATA/TCE as mapped out by DSC; (O) gel melting, (+) gel formation; the solid line and the dotted line are fits with an arbitrary function* ($T = a - b \times c^{X_{TATA}}$). *The Tamman's plot is also given on top with same meaning for the symbols.Here the linear variation is theoretically expected. b)* ***right****: PVC/TCE gel melting (●) as obtained by DSC, gel formation as obtained by the tube tilting method (●) solid lines are fits with an arbitrary function* ($T = aLn(-bLnX_{TATA})$). *In the case of the gel melting errors bars indicate the melting range, while those on cooling stand for the uncertainty on the gel formation determination.*

of 1.66 between the first and the second reflection close to $\sqrt{3}$ may suggest a frustrated structure [30,31]

2) The binary systems in tetrachlorethane (TCE).

Typical DSC traces are shown in figure 2b. The temperature-concentration phase diagram drawn in figure 4a for TATA/TCE gels has been mapped out by DSC for heating and cooling rates of 5°C/min. Formation and melting temperatures are monotonously increasing with TATA

concentration. A fit is carried out with an adequate function of no theoretical meaning as a guide for the eyes and for use in the case of the ternary system ($T = a - b \times c^{X_{TATA}}$). The Tamman's diagram drawn on top reveals a linear variation of the enthalpies with concentration as theoretically expected by the lever rule. The melting enthalpies and formation enthalpies are the same for the same concentration, which highlights that kinetic effects are absent, namely gel formation is instantaneous. Extrapolation to X_{TATA}= 1 yields ΔH= 39 J/g, a value smaller than that measured on the solid sample for the terminal melting but higher than that related to the solid-solid transformation at T= 198°C (see figure 2a). These discrepancies indicate a different molecular structure as will be confirmed below.

As has been reported in several papers [24,25] the determination of the gelation temperature of PVC solutions turns out to be impossible as the formation exotherms are not detectable. Only the melting range can be determined on the first heating, yet the associated enthalpy is meaningless being chiefly artefactual (see figures S1 for further explanations). The gelation temperatures have then been measured by the tube tilting method (see sup. info figure S2). The results reported in figure 4b are also fitted with an arbitrary function as a guide for the eyes ($T = aLn(-bLnX_{TATA})$).

The diffraction patterns obtained on TATA/TCE xerogels are shown in figure 5a. The use of xerogels instead of wet gels is required on account of the high chlorine content that causes virtual, total X-ray absorption. Admittedly, this leaves the question unresolved as to whether the structure observed on the xerogel pertains to that in the wet gel. Here, the xerogels were simply prepared by solvent evaporation at room temperature.

The TATA/TCE pattern displays the typical reflections at 0.49 and 0.47 associated to the helix elevation and to the phenyl-phenyl distance [16], respectively (figure 5a). Only one broad peak is seen at low q (q= 2.13 nm^{-1} and d= 2.95 nm). The full width at half maximum is determined by a fit with a Lorentzian function after subtraction of a background intensity corresponding to the scattering of the PVC+TATA (figure 5b and see sup. info. figure S4 for details). In this aim, the Debye-Bueche two-density model is used [32]:

$$I_o(q) = A + \frac{B}{[1+(q\sigma)^4]} \quad (1)$$

where A is a residual background, and σ a characteristic distance. The peak broadening is FWHM= 1.1, and the associated correlation length ξ= 2π/FWHM≈ 5.7 nm.

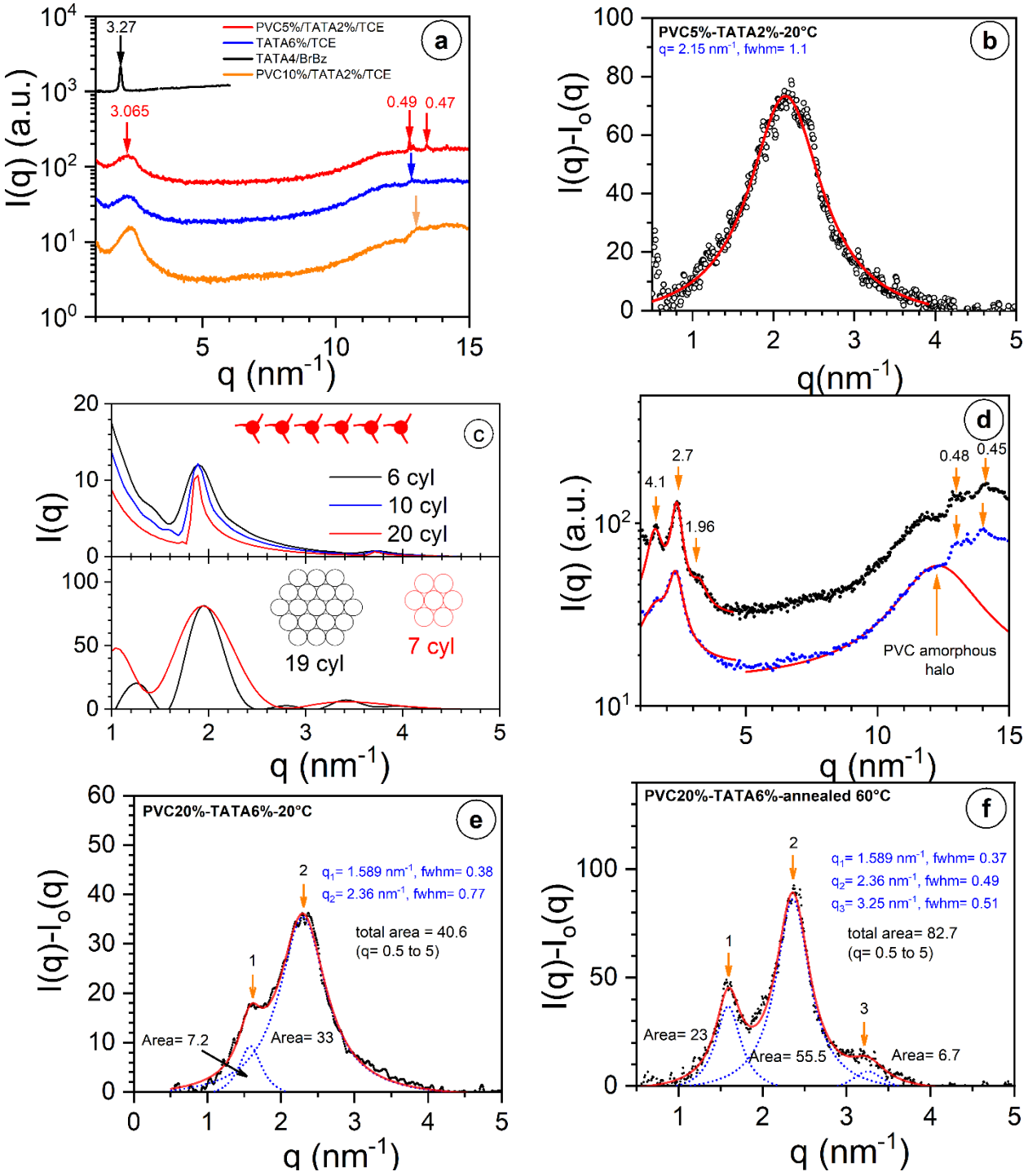

Figure 5: *Diffraction patterns of xerogels; in all experimental plots red solid lines are fits with Lorentzian functions a)* ***upper left:*** *PVC5%/TATA2%/TCE and PVC10%/TATA2%/TCE, TATA6%/TCE and TATA4%/bromobenzene (see legend in the figure; b)* ***upper right****: focus on the peak at q= 2.15 nm^{-1} after background subtraction (see text); c)* ***middle left:*** *theoretical curves for hexagonal packing and for arrangement in a row. d)* ***middle right:*** *PVC20%/TATA/TCE. (●) gel dried at 20°C; (●) gel heated-dried at 60°C; distances as indicated. e)* ***Bottom left:*** *focus on the low-q peaks for gel dried at 20°C after background subtraction, peaks are decomposed by Lorentzian functions (blue dotted lines); f)* ***bottom right:*** *idem gel heated-dried at 60°C.*

In figure 5a, the diffraction pattern obtained on a TATA/bromobenzene in a previous paper is also shown in the low-q range. Here, the peak is far much narrower as the FWHM= 0.08, which gives $\xi \approx$ 78 nm. Admittedly, the molecular organization differs whether gels are prepared in tetrachlorethane or in bromobenzene, but also is far less extended than in the solid state. As these peaks are in the low-q range, the intensity scattered by TATA helices can be approximated to the equivalent cylinder where they are inscribed [33]. Due to the difference in electron density (see figure 1), one has actually to consider two concentric cylinders with different scattering amplitudes. One is therefore a solid cylinder while the other is a hollow cylinder. The intensity then reads [34]:

$$I(q) \sim \frac{\pi \mu_L}{q}\left[\frac{2A_{in}}{A_m q r_{out}} J_1 q\gamma r_{out} + \frac{2A_{out}}{A_m q r_{out}} \times \{J_1(q r_{out}) - \gamma J_1(q\gamma r_{out})\}\right]^2 \times \sum_{j=1}^{n}\sum_{k=1}^{n} J_o(q d_{jk}) \quad (2)$$

where A_{in}, A_{out} and r_{in} the radius of the inner cylinder, and r_{out} are the scattering amplitudes and the radii of the inner cylinder and of the outer hollow cylinder, respectively, with $\gamma = r_{in}/r_{out}$, and $A_m = \gamma^2 A_{in} + [1-\gamma^2]A_{out}$, with $A_{in}/A_{out} = 4.03$, d_{jk} the distance between the axis of cylinders j and k, n the number of cylinders, and J_1 and J_o Bessel functions of first type and order 1 and 0.

In equation 2 the left member corresponds to the helix scattering [35,36] while the right member stands for the intermolecular terms [34]. Two types of helix organization have been contemplated: *hexagonal packing* with 7 and 19 helices, and *helices arranged in a row* (figure 5c).

In the case of the hexagonal packing the following values have been used for reproducing the peak at the desired position: r_{out}= 1.95 nm and the distance between two adjacent cylinders d= 3.5. The case of an assembly of 7 cylinders reproduces reasonably well the diffraction curve for TATA/TCE systems to a first approximation while introducing a higher number of cylinders entails the appearance of new peaks. The FWHM value is relatively close to what is experimentally measured. Conversely, this parameter does not change significantly when increasing the number of cylinders from 7 to 19 and is far from the experimental value determined for the TATA/Bromobenzene gels.

Alternatively, the diffraction pattern observed for TATA/Bromobenzene gels is best fitted by considering helices arranged in a row with r_{out}= 2 nm, and d= 3.4 nm the distance between adjacent helices (figure 5c). Here, the FWHM value decreases drastically with the increasing number of

cylinders (0.52 for 6 helices, 0.34 for 10 helices and 0.17 for 20 helices). The absence of additional diffraction peaks, and correspondingly of intermolecular terms, implies that adjacent rows are not spatially correlated. It can be assumed that decorrelation is possibly achieved by randomly intercalation of solvent molecules as portrayed in figure 3b.

3) The ternary systems PVC/TATA in tetrachlorethane (TCE).

As the thermal events from the PVC moiety are not observable, only the melting and formation temperatures of the TATA molecules are investigated and compared to those determined in their binary gels. Two types of behaviour have been observed depending upon the PVC composition, namely results in systems containing 5 to 10% PVC (low PVC content) differ drastically from those obtained for 20% to 30%PVC (high PVC content).

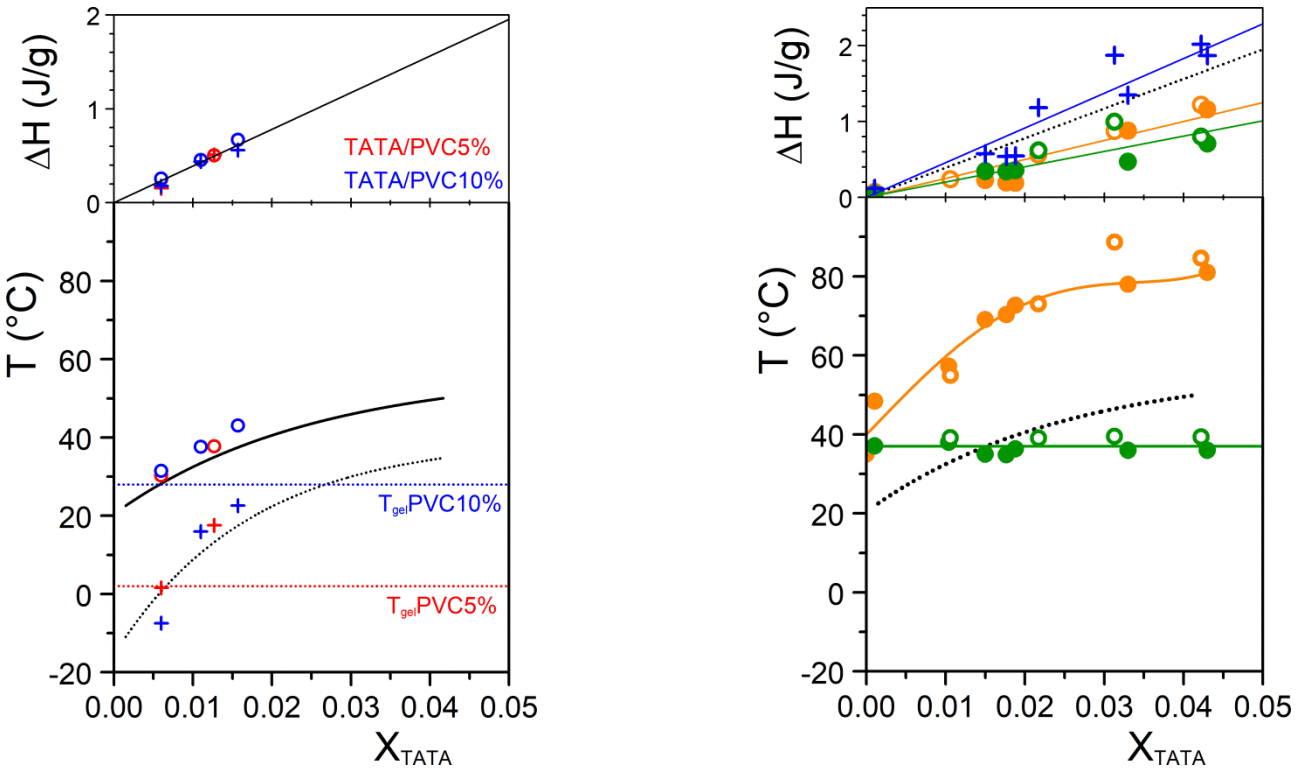

Figure 6: *2D temperature-concentration phase diagram PVC/TATA/TCE as mapped out by DSC;* ***a) Left****: (○,○) gel melting, (+, +) gel formation for PVC10% and PVC 5%, respectively; ; the solid line and the dotted line stand for the melting and the formation of the TATA/TCE binary gels. The formation temperatures of PVC binary gels are shown dotted lines. The Tamman's diagram is shown on top. b)* ***right****: (●,○) terminal gel melting, (●,○) gel transformation for PVC20% and PVC30%, respectively; the orange solid line is a fit with a polynomial of degree 4, the green solid line is a theoretical fit with a straight line of slope 0 (non-variant event). The dotted line= melting of the binary gels Top Tamman's diagram with the same meaning for the symbols. The blue crosses stand for the sum of the enthalpies of the gel transformation and the gel melting.*

a) low PVC content (PVC5% and PVC10%)

For the sake of simplicity, only the 2D temperature-concentration phase diagram mapped out by DSC for the TATA moiety is drawn in figure 6a. As can be seen, the melting and formation temperatures differ only slightly from those determined on the binary systems.

In view of the T-C phase diagram for the binary systems, TATA fibrils are supposed to form first and then PVC gel for the ternary system PVC5%/TATA/TCE. Yet, for the PVC10%/TATA/TCE ternary system, TATA fibrils grow within the already present PVC network. In any case, this does not alter significantly the TATA thermodynamic properties (see figure 5d), nor does it modify the molecular organization as the diffraction patterns are virtually identical to that observed for the binary TATA system. Here again, the xerogels were simply prepared by solvent evaporation at room temperature.

Alternatively, the morphology of the ternary gels depends upon the composition in PVC (figure 7c to 7f). For PVC5%/TATA/TCE one can clearly see that the TATA fibrils are randomly dispersed within the PVC gel matrix (figure 7c). The cross-section of the TATA fibrils, 150 nm, are within the range observed in the binary system, 70-400 nm. This is consistent with the fact that TATA fibrils grow first, and then the PVC gel pervades the remaining space.

Conversely, for PVC10%/TATA/TCE ternary gels, the dispersion of the TATA fibrils is different (figure 7d). Their density is lower while their cross-sections of about 1200 nm are significantly larger. This may arise from the fact that this time the TATA fibrils grow within the existing PVC gel. Yet, as shown above by X-ray diffraction, this does not modify the molecular organization.

b) high PVC content (PVC20% and PVC30%)

Further increase of the PVC composition modifies totally the thermodynamic behaviour of the TATA moiety. A typical DSC thermogram is shown in figure 2b whose shape is at variance with those obtained previously. A sharp peak occurs first, then followed by a broader endotherm. The resulting 2D temperature-concentration phase diagram also differs drastically from that obtained at 5% and 10% PVC compositions (figure 6b). Two remarkable features are seen: i) the liquidus line,

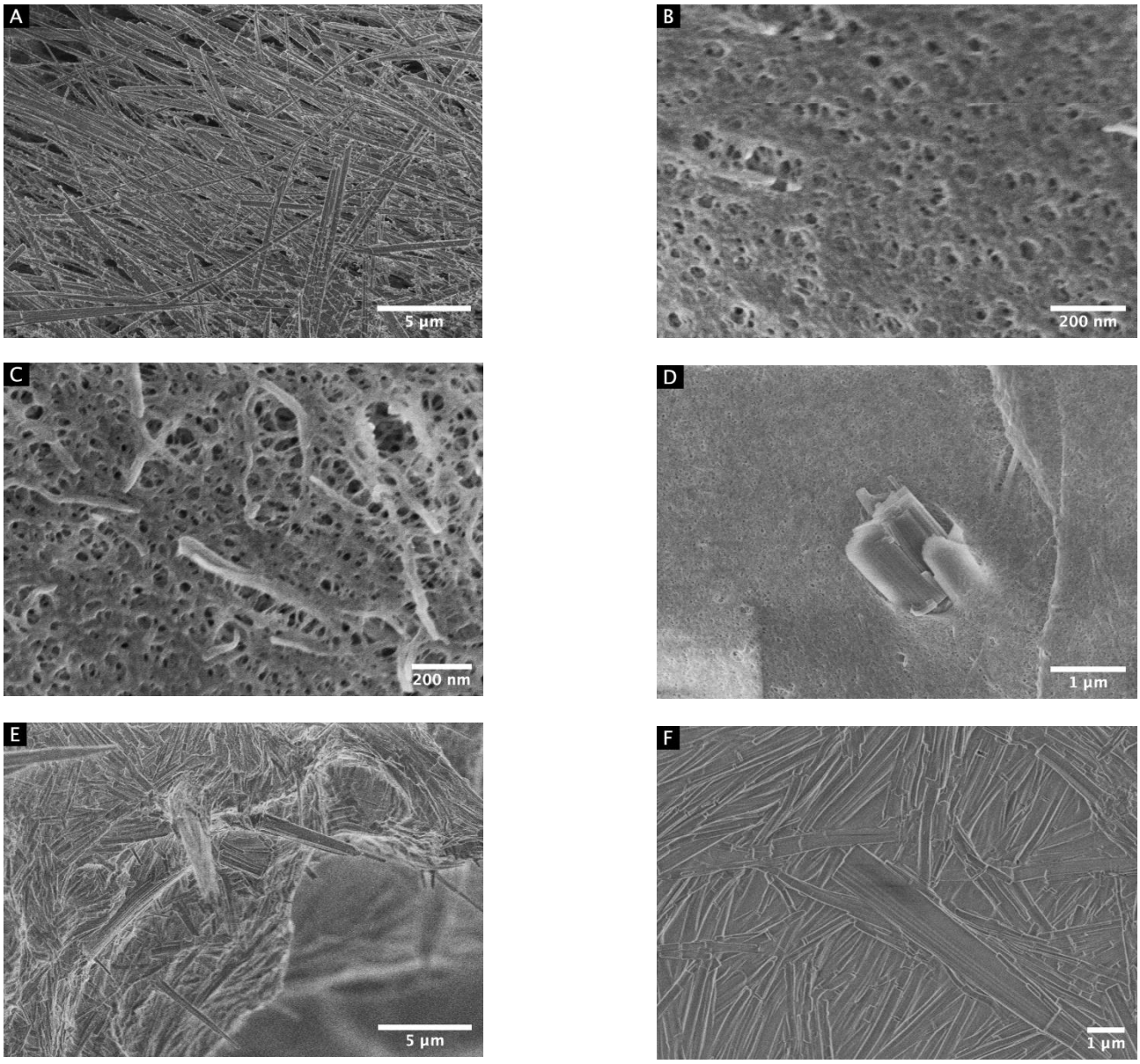

Figure 7: *Gel morphology from cryoSEM investigations. A) Upper left= TATA1%/TCE; B) upper right= PVC10% gel; C) middle left= PVC5%/TATA1%/TCE, TATA fibrils and the PVC gel are highlighted; D) middle right= PVC10%/TATA2%. E) Lower left and F) lower right= PVC30%/TATA3%.*

namely the terminal melting of the TATA fibrils, shifts towards higher temperatures, and ii) a non-variant transformation of the solid-solid type takes place at T= 37±2°C. Note that this transition is not related to that observed in the solid state.

As can be seen in figure 5d the diffraction patterns also point to a different molecular organization than that observed in the TATA binary gel and in gels of low PVC content. Here, the xerogels were prepared by solvent evaporation in two ways: to determine the structure below 37°C the sample

were obtained by simple evaporation at room temperature, while for determining the structure above 37°C the samples were first heated at 50°C and then dried at this temperature (labelled as *heated-dried*).

After subtraction of the amorphous background by means of equation1, one can determine in the low-q range two peaks at q_1= 1.589 nm^{-1} (d_1= 3.95 nm) and q_2= 2.36 nm^{-1} (d_2= 2.66 nm) for samples dried at 20°C (figure 5e). For samples heated-dried at 60°C the diffraction pattern exhibits three peaks at q_1= 1.589 nm^{-1} (d_1= 3.95 nm), q_2= 2.36 nm^{-1} (d_2= 2.66 nm), and q_3= 3.25 nm^{-1} (d_3= 1.93 nm) (figure 5f). In the high-q range, one retrieves the peak at d= 0.48 and d= 0.45 related to the helical structure, which therefore remains unchanged despite the differing 2D packing.

These results confirm the occurrence of a 1st order phase transition as has been inferred from the temperature-concentration phase diagram. Again, this transformation is not related to that observed in the solid state but rather relates to a transformation of a molecular compound either in another less-solvated compound or a solid phase.

The high PVC content therefore produces a molecular organization that displays reflections located at positions virtually identical to those reported for structure I, although the intensity differs for the peak at q_1= 1.589 nm^{-1} (see figure 3a). This suggests that the formation of a TATA/solvent molecular compound is a plausible assumption that would be consistent with the 1st order phase transition observed at T= 37°C, together with the variation of peak intensity. These molecular compounds would rather be of the clathrate type [37,38] as there are channels large enough in between the TATA helices independent of the way they laterally pack.

The gel morphology also differs from that observed for low PVC content (figure 7e and 7f). The PVC network cannot be distinguished, something expected as its mesh size usually varies as ($C^{-1/3}$) [25], which suggest a value around 5 nm in the present case (i.e. C= 0.246 g/cm^3) as deduced from the values observed at C= 9.3×10^{-2} g/cm^3 (figure 7b). TATA fibrils chiefly display two highly regular aspects: either flat laths or elongated needles. Their cross-sectional size is about the same as those observed in the TATA binary system. It is worth emphasizing that despite a limited molecular

organization the TATA fibrils possess highly regular shapes well beyond the correlation lengths derived from the X-ray data.

CONCLUDING REMARKS

Results reported here show a variety of thermodynamic behaviour as well as a diversity of molecular arrangements of the TATA molecules. As much as 6 different packing structures are seen, 3 in the solid state and 3 in the gel states. The issue of the involvement of the solvent molecules in the latter still remains a challenge, the more so as the number of X-ray reflections is limited. Neutron diffraction experiments are clearly the appropriate tool that allows one to study these systems in the wet state. Two problems can be overcome: i) as chlorine atoms do not absorb neutrons to the same extent as X-ray photons do, studies can be performed in highly chlorinated solvents without prior drying, and ii) the diffraction pattern depends upon the solvent labelling as has been shown in the case of polymer-solvent molecular compounds [39,40]. Whether the diffraction pattern is either modified or not modified by using hydrogenous or deuterated solvent, can clearly demonstrate the occurrence or the absence of a molecular compound.

The thermodynamic properties of the TATA/TCE system are totally altered by addition of PVC, a covalent polymer. High PVC concentrations increase the TATA terminal melting but also generate a non-variant transformation that may well be related to an incongruently-melting compound[3]. Evidently, the thermodynamic and the molecular structures point towards a role of the solvent other than a mere diluent.

Supporting information:

Sol-Gel determination, diffraction patterns with indexations, signal processing for the diffraction peaks.

Acknowledgments: The authors are indebted to G. Fleith for experimental assistance in X-ray diffraction experiments, and C. Saettel for DSC measurement data acquisition.

Conflict of interest: The authors declare no conflict of interest.

REFERENCES

1) see for instance *Additives in Polymers: Analysis and Applications* Eds. A. A. Berlin, S. Z. Rogovina, G. E. Zaikov, 364p, **2021**, Apple Academic Press, CRC press

2) *Molecular Gels: Materials with Self-Assembled Fibrillar Networks* Terech, P.; Weiss, R.G., Editors, Springer Verlag, 2006

3) Guenet, J.M. Organogels: thermodynamics, structure, solvent role and properties**, 2016**, N.Y., Springer International Publishing

4) *Molecular Gels, Structure and Dynamics*, Weiss, R.G. Ed., Monograph in Supramolecular Chemistry, **2018**, Royal Society of Chemistry, London

5) Dasgupta, D.; Srinivasan, S.; Rochas, C.; Ajayaghosh, A.; Guenet, J.M. Hybrid thermoreversible gels from covalent polymers and organogels *Langmuir* **2009**, *25*, 8593;

6) Dasgupta, D.; Kamar, Z.; Rochas, C.; Dahmani, M.; Mesini P., Guenet, J.M. Design of hybrid networks by sheathing polymer fibrils with self-assembled nanotubules *Soft Matter*, **2010**, *6*, 3573.

7) Raj, G.; Boulaoued, A.; Lacava, J.; Biniek, L.; M´esini, P.J.: Brinkmann, M.; Faure-Vincent, J.; Guenet, J.M. Insulated Molecular Wires: Sheathing Semiconducting Polymers with Organic Nanotubes through Heterogeneous Nucleation *Adv. Electron. Mater.* **2017**, *3*, 1600370

8) Boulaoued, A.; Bantignies, J.L.; Le Parc, R.; Goze-Bac, C.; Mesini, P.;. Nguyen, T.T.T.; Al Ouahabi, A.; Lutz, P.; Guenet, J.M. Hybrid Fibrillar Xerogels with Unusual Magnetic Properties, *Langmuir* **2016**, *32*, 13193

9) Zoukal, Z.; Elhasri, S.; Carvalho, A.; Schmutz, M.; Collin, D.; Vakayil, P.K.; Ajayaghosh, A.;Guenet, J.M. Hybrid materials from poly[vinyl chloride] and organogels *ACS Appl. Polym. Mater.* **2019**, *1*, 1203

10) Guenet, J.M. Hybrid Physical Gels from Polymers and Self-Assembled Systems: A Novel Path for Making Functional Materials *Gels* **2018**, *4*, 35

11) Ellis, T. K.; Galerne, M.; Armao IV, J. J.; Osypenko, A.; Martel, D.; Maaloum, M.; Fuks, G.; Gavat, O.; Moulin, E.; Giuseppone, N. Supramolecular electropolymerization *Angew. Chem. Int.*

Ed. **2018**, *57*, 15749-15753.

12) Moulin, E.; Niess, F.; Maaloum, M.; Buhler, E.; Nyrkova, I. ; Giuseppone, N. The hierarchical self-assembly of charge nanocarriers: a highly cooperative process promoted by visible light *Angew. Chem. Int. Ed.* **2010**, *49*, 6974.

13) Eric Busseron, E.; Cid, J.J.; Wolf, A.; Du, G.; Moulin, E.; Fuks, G.; Maaloum, M.; Polavarapu, P.; Ruff, A.; Saur, A.K.; Ludwigs, S.; Giuseppone, N. Light-Controlled Morphologies of Self-Assembled Triarylamine-Fullerene Conjugates *ACS Nano* **2015**, *9*, 2760

14) Nyrkova, I. ; Moulin, E.; Armao IV, J.J.; Maaloum, M.; Heinrich, B.; Rawiso, M.; Niess, F.; Cid, J.J.; Jouault, N.; Buhler, E.; Semenov, A. Giuseppone, N. Supramolecular self-assembly and radical kinetics in conducting self-replicating nanowires. *ACS Nano* **2014**, *8*, 10111;

15) Picini, P.; Schneider, S. ; Gavat, O. ;Vargas Jentzsch, A. ;Tan, J. ; Maaloum, M. ; Strub, J.M. ; Tokunaga, S. ; Lehn, J.M. ; Moulin, E. ; Giuseppone, N. Supramolecular Polymerization of Triarylamine-Based Macrocycles into Electroactive Nanotubes *J. Am. Chem. Soc.* **2021**, *143*, 6498

16) Armao IV, J.J.; Maaloum, M.; Ellis, T.; Fuks, G.; Rawiso, M.; Moulin,E.; Giuseppone, N. Healable supramolecular polymers as organic metals *J. Am. Chem. Soc*. **2014**, *136*, 11382

17) Moulin,E.; Armao IV, J.J.; Giuseppone, N. Triaryl amine-based supramolecular polymers: structure, dynamics, and functions *Acc. Chem. Res.* **2019**, *52*, 975

18) See for instance Gnanou, Y.; Fontanille, M. *Organic and Physical Chemistry of Polymers*, **2008** John Wiley & Sons, N.Y.

19) Stein, R.S.; Tobolsky, A.V. An investigation of the relationship between polymer structure and mechanical properties: Part II: An Experimental Study of the Stress and Birefringence Properties *Text. Res. J.* **1949**, *18*, 302

20) Alfrey, T.; Wiederhorn, N.; Stein, R.S.; Tobolsky, A.V. Some studies of plasticized polyvinylchloride *J. Colloid. Sci.* **1949**, *4*, 211.

21) Walter, A.T. Elastic properties of polvinyl chloride gels *J. Pol. Sci.* **1954**, *13*, 207

22) Juijn, J.A.; Gisolf, A.; de Jong, W.A. Crystallinity in atactic poly vinyl chloride *Kolloid Z. Z. Polym*. **1973**, *251*, 456

23) te Nijenhuis, K., Dijkstra, H. Investigation of the aging process of a polyvinyl chloride gel by the measurement of its dynamic moduli *Rheol. Acta* **1975**, *14*, 71.

24) Yang, Y.C. and Geil, P.H. Morphology and properties of PVC/solvent gels *J. Macromol. Sci.* **1983**, *B(22)*, 463

25) Mutin, P.H.; Guenet, J.M. Physical gels from PVC: ageing and solvent effect on thermal behavior, swelling and compression modulus. *Macromolecules* **1989**, *22*, 843.

26) M. Galerne PhD thesis «Etude de la relation structure-propriétés de polymères supramoléculaires de triarylamines» Strasbourg university 2020

27) Natta, G, Corradini, P. Structure and properties of isotactic polypropylene *Suppl. Nuevo Cim.* **1960**, *10*, 40

28) Natta, G, Corradini, P., Bassi, I.W. Crystal structure of isotactic polystyrene *Suppl. Nuevo Cim.* **1960**, *15*, 68

29) Guerra, G.; Manfredi, C.; Musto, P.; Tavone, S. Guest conformation and diffusion into amorphous and emptied clathrate phases of syndiotactic polystyrene *Macromolecules* **1998**, *31*, 1329

30) Toulouse, G.Theory of the frustration effect in spin glasses *Commun. Phys*. **1977**, *3*, 115.

31) Lotz, B.L. Frustration and Frustrated Crystal Structures of Polymers and Biopolymers *Macromolecules* **2012**, *45*, 2175

32) Debye, P. and Bueche, A.M. *J. Appl. Phys*. **1949** *20* 518

33) Pringle, O.A., Schmidt, P.W. Small-Angle X-Ray Scattering from Helical Macromolecules *J. Appl. Cryst.*, **1971**,*4*, 290

34) Oster, G., Riley, D.P. Scattering from Cylindrically Symmetric Systems *Acta Cryst*., **1952**, *5*, 272

35) Mittelbach, P., Porod G. Zur Röntgenkleinwinkelstreuung verdünnter kolloiden Systeme *Acta Physica Austriaca,* **1961**, *14*, 185

36) Saiani, A.; Gunete, J.M. Nanostructure and Helicity in Syndiotactic Poly(methyl methacrylate) Thermoreversible Gels *Macromolecules* **1999**, *32*, 657

37) Tadokoro, H.; Chatani, Y.; Yoshihara, T.; Tahara, S.; Murahashi, S. Structural studies on polyethers, [- (CH2)m- O-]n. II. Molecular structure of polyethylene oxide *Makromol. Chem.* **1964**, *73*, 109

37) Chenite, A.; Brisse, F.; Structure and conformation of poly(ethylene oxide), PEO, in the trigonal form of the PEO-urea complex at 173 K *Macromolecules* **1991**, *24* 2221

38) Daniel C.; Menelle, A.; Brulet, A.; Guenet, J.M. Thermoreversible Gelation of Syndiotactic Polystyrene in Toluene and Chloroform *Polymer* **1997**, *38*, 4193

39) Kaneko, F.; Seto, N.; Sato, S.; Radulescu, A.; Schiavone, M.M.; Allgaier, J.; Ute, K. Development of a Simultaneous SANS/FTIR Measuring System *Chemistry Letters*, **2015**, *44*, 497